



## Article

# Surface-Enhanced Raman Spectroscopic Investigation of PAHs at a Fe<sub>3</sub>O<sub>4</sub>@GO@Ag@PDA Composite Substrates

Junyu Liu <sup>1,2</sup>, Wencan Cui <sup>3</sup>, Shihua Sang <sup>1,\*</sup>, Liang Guan <sup>2,\*</sup>, Kecheng Gu <sup>2,\*</sup>, Yinyin Wang <sup>2</sup> and Jian Wang <sup>2</sup>

<sup>1</sup> College of Material and Chemistry & Chemical Engineering, Chengdu University of Technology, Chengdu 610059, China

<sup>2</sup> Department of Petroleum, Oil and Lubricants Army Logistics Academy of PLA, Chongqing 401331, China

<sup>3</sup> Department of Basic Courses, Army Logistic Academy of PLA, Chongqing 401331, China

\* Correspondence: sangsh11@163.com (S.S.); gl\_200122@163.com (L.G.); gukecheng130521@163.com (K.G.)

**Abstract:** A method for surface-enhanced Raman spectroscopy (SERS) sensing of polycyclic aromatic hydrocarbons (PAHs) is reported. Fe<sub>3</sub>O<sub>4</sub>@PDA@Ag@GO is developed as the SERS substrate prepared by classical electrostatic attraction method based on the enrichment of organic compounds by graphene oxide (GO) and polydopamine (PDA) and the good separation and enrichment function of Fe<sub>3</sub>O<sub>4</sub>. The morphology and structure of the SERS substrate were represented by transmission electron microscopy (TEM), energy-dispersive spectroscopy (EDS), X-ray diffraction (XRD) and the UV–visible absorption spectrum (UV–vis spectra). The effect of different temperatures on SERS during synthesis was investigated, and it was found that the best effect was achieved when the synthesis temperature was 90 °C. The effect of each component of Fe<sub>3</sub>O<sub>4</sub>@PDA@Ag@GO nanocomposites on SERS was explored, and it was found that Ag NPs are of great significance to enhance the Raman signal based on the electromagnetic enhancement mechanism; apart from enriching the polycyclic aromatic hydrocarbons (PAHs) through  $\pi$ – $\pi$  interaction, GO also generates strong chemical enhancement to the Raman signal, and PDA can prevent Ag from shedding and agglomeration. The existence of Fe<sub>3</sub>O<sub>4</sub> is favored for the fast separation of substrate from the solutions, which greatly simplifies the detection procedure and facilitates the cycle use of the substrate. The experimental procedure is simplified, and the substrate is reused easily. Three kinds of PAHs (phenanthrene, pyrene and benzanthene) are employed as probe molecules to verify the performance of the composite SERS substrate. The results show that the limit of detection (LOD) of phenanthrene pyrene and benzanthene detected by Fe<sub>3</sub>O<sub>4</sub>@PDA@Ag@GO composite substrate are 10<sup>−8</sup> g/L (5.6 × 10<sup>−11</sup> mol/L), 10<sup>−7</sup> g/L (4.9 × 10<sup>−10</sup> mol/L) and 10<sup>−7</sup> g/L (4.4 × 10<sup>−10</sup> mol/L), respectively, which is much lower than that of ordinary Raman, and it is promising for its application in the enrichment detection of trace PAHs in the environment.



**Citation:** Liu, J.; Cui, W.; Sang, S.; Guan, L.; Gu, K.; Wang, Y.; Wang, J. Surface-Enhanced Raman Spectroscopic Investigation of PAHs at a Fe<sub>3</sub>O<sub>4</sub>@GO@Ag@PDA Composite Substrates. *Micromachines* **2022**, *13*, 1253. <https://doi.org/10.3390/mi13081253>

Received: 23 June 2022

Accepted: 1 August 2022

Published: 4 August 2022

**Publisher's Note:** MDPI stays neutral with regard to jurisdictional claims in published maps and institutional affiliations.



**Copyright:** © 2022 by the authors. Licensee MDPI, Basel, Switzerland. This article is an open access article distributed under the terms and conditions of the Creative Commons Attribution (CC BY) license (<https://creativecommons.org/licenses/by/4.0/>).

**Keywords:** surface-enhanced Raman spectroscopy; composite substrate; Ag; PAHs; enrichment detection

## 1. Introduction

Polycyclic aromatic hydrocarbons, which are widespread in the environment, are a kind of hydrocarbon containing two or more conjoined aromatic rings [1]. PAHs are mainly produced during the incomplete combustion of organic matter. Their carcinogenic, teratogenic and mutagenic effects are great threats to human health [2–5]. Nsibandé et al. summarized the concentration of polycyclic aromatic hydrocarbons in various waters between 10<sup>−6</sup>–10<sup>−11</sup> mol/L [6].

Therefore, the monitoring of the content and types of PAHs in the environment has attracted extensive attention. The detection methods for PAHs, such as gas chromatography, high-performance liquid chromatography (HPLC), gas chromatography-mass spectrometry (GC-MS), nuclear magnetic resonance (NMR) [7–13], etc., are accurate and used widely. Although the detection methods mentioned above have high sensitivity and stability,

they usually demand expensive instrument and complex pre-treatment and enrichment processes, which are time-consuming. These shortcomings bring difficulties to the universal application of these methods. Therefore, a rapid and economical method with high-sensitivity and high-selectivity for PAH detection is necessary.

As an analytical technique with high sensitivity and strong feature recognition ability, surface-enhanced Raman spectroscopy (SERS) has been used widely in rapid detection [14–18]. According to the SERS enhancement mechanism, the target molecules must usually adsorb onto the surface of the SERS substrate by physical or chemical means or be in a short effective enhancement range. However, it is difficult to detect SERS substrates by conventional methods [16] because hydrocarbons such as PAHs do not have special functional groups that interact with metal substrates. Especially when the content of SERS is low, the difficulty of detection increases significantly. Therefore, surface functionalization of SERS substrate is necessary. At present, nanomaterials of noble metals (Au and Ag), transition metals and non-metallic graphene are mainly used to prepare substrates [19–31].

Currently, one of the most used methods mainly focuses on fixing PAH molecules on SERS substrate surfaces by self-assembly layer modification. For example, Harris et al. modified the metal substrate with the substitution of C18, and, with the help of portable Raman spectrometer, SERS detection of polycyclic aromatic hydrocarbon molecules pyrene and phenanthrene was carried out, with detection limits of  $10^{-8}$  mol/L and  $10^{-7}$  mol/L, respectively [32]. Jones et al. and Costa et al. assembled a layer of mercaptan molecules on Ag and Au membrane substrates by self-assembly. The minimum concentrations detected by pyrene are  $7 \times 10^{-10}$  mol/L [31,33]. The ability of SERS substrate to capture PAH molecules was improved. Through the improvement of nanoparticles, Jing et al. and Wang et al. prepared  $\text{Fe}_3\text{O}_4$ @Ag magnetic nanoparticles modified by thiol molecules and “bowl-shaped” Ag substrates modified by thiol, respectively, realizing the highly sensitive detection of PAHs molecules [34,35]. Wang et al. prepared an Ag-nanoparticle–graphene hybrid for the direct detection of PAHs. The synthesis process is relatively simple, and the raw materials are not expensive, while the limit of detection for pyrene, phenanthrene are as low as 0.73 ppb and 0.57 ppb, respectively [36].

Although this method has achieved SERS detection of PAHs, the organic molecules used for modification are usually difficult to synthesize, which limits the application of SERS.

Until now, the combination of  $\text{Fe}_3\text{O}_4$ , PDA, GO and Ag as a SERS substrate for the detection of PAHs has not been reported. PDA is a substance with rich functional groups, good hydrophilicity and excellent biocompatibility, which can cover many organic and inorganic materials such as magnetic nanomaterial  $\text{Fe}_3\text{O}_4$ . The existence of  $\text{Fe}_3\text{O}_4$  can separate the substrate quickly and simplify the experimental steps. Graphene oxide (GO) is also known as functional graphene which has a two-dimensional spatial structure and is a carbon-based nanomaterial with abundant hydroxyl, epoxy, carboxyl and other oxygen-containing energy groups. It has high specific surface energy, good hydrophilic and mechanical properties and good adsorption of many chemicals. The accumulation and hydrophobic action of  $\pi$ - $\pi$  between GO and PAHs can be used to enable the PAHs to show a strong enrichment ability. Ag and GO enhances the Raman signal in  $\text{Fe}_3\text{O}_4$ @PDA@Ag@GO substrate. PDA has good adhesion and reactivity. The composite nanoparticles have good magnetic response, which can quickly separate and enrich the molecules to be measured and shorten the pretreatment time.

In this study,  $\text{Fe}_3\text{O}_4$ @PDA@Ag@GO composite material was synthesized by assembly method to detect phenanthrene, pyrene and benzoanthracene in aqueous solution. The limit of detection for phenanthrene, pyrene and benzoanthracene are  $10^{-8}$  g/L ( $5.6 \times 10^{-11}$  mol/L),  $10^{-7}$  g/L ( $4.9 \times 10^{-10}$  mol/L) and  $10^{-7}$  g/L ( $4.4 \times 10^{-10}$  mol/L), respectively, which is much lower than that of ordinary Raman (Wang et al. prepared an Ag-nanoparticle/graphene hybrid for the direct detection of PAHs. The limit of detection for phenanthrene is 3.2 nM (~0.57 ppb) [24]). Our team synthesized  $\text{Fe}_3\text{O}_4$ @PDA@Au@GO substrate for the detection of phenanthrene. The limit of detection (LOD) of phenanthrene is  $10^{-7}$  g/L.

The raw materials for Fe<sub>3</sub>O<sub>4</sub>@PDA@Ag@GO substrates are much cheaper than those of Fe<sub>3</sub>O<sub>4</sub>@PDA@Au@GO.

## 2. Experimental

### 2.1. Materials and Apparatus

Materials and apparatus used in the experiment are shown in the following Tables 1 and 2:

**Table 1.** Reagents.

Reagent	Grade	Manufacturer
Ethylene glycol	analytical purity	Chengdu Colon Chemicals Co., Ltd. (Chengdu, China)
Methanol	analytical purity	Chengdu Colon Chemicals Co., Ltd. (Chengdu, China)
Anhydrous ethanol	analytical purity	Chengdu Colon Chemicals Co., Ltd. (Chengdu, China)
Polyethylene glycol	analytical purity	Beijing Chemical Reagent Co., Ltd. (Beijing, China)
Ferric chloride hexahydrate	analytical purity	Beijing Chemical Reagent Co., Ltd. (Beijing, China)
Silver nitrate	analytical purity	Beijing Chemical Reagent Co., Ltd. (Beijing, China)
Sodium citrate	analytical purity	Beijing Chemical Reagent Co., Ltd. (Beijing, China)
Phenanthrene	analytical purity	McLean Biochemical Technology Co., Ltd. (Shanghai, China)
Pyrene	analytical purity	McLean Biochemical Technology Co., Ltd. (Shanghai, China)
Benzanthracene	analytical purity	McLean Biochemical Technology Co., Ltd. (Shanghai, China)
Graphene oxide dispersion	0.5 mg/mL	Beijing Chemical Reagent Co., Ltd. (Beijing, China)
Hydrochloric acid-dopamine	analytical purity	McLean Biochemical Technology Co., Ltd. (Shanghai, China)
Anhydrous sodium acetate	analytical purity	Beijing Chemical Reagent Co., Ltd. (Beijing, China)

**Table 2.** Laboratory apparatus.

Apparatus Names	Manufacturers	Model Number
Electronic balances	METTLER TOLEDO, Zurich, Switzerland.	XP5003S
Thermostatic magnetic agitator	Jintan Fuhua Electric Appliance Co., Ltd.	RCT B S25
TG16-WS high speed centrifuge	Hunan Xiangyi Laboratory Instrument Development Co., Ltd.	TG16-WS
SB-5200DT Ultrasonic cleaner	Ningbo Xinzhi Biotechnology Co., Ltd.	SB-5200DT
Metage Opal 2800 spectrometer	Metage Co., London, England	Metage Opal 2800
50mL Stainless steel reactor	Chengdu Cologne Chemicals Co., Ltd.	PDFE
DZF vacuum oven	Beijing Yongguangming Medical Instrument Co., Ltd.	DZF
Electric blower drying box	Chongqing Star Test Equipment Co., Ltd.	CS101-2EB
Spectrophotometer	Shanghai Meipuda Instrument Co., Ltd.	UV-1600PC

### 2.2. Material Synthesis

#### 2.2.1. Synthesis of Fe<sub>3</sub>O<sub>4</sub> Nanoparticles

A total of 0.9 g of FeCl<sub>3</sub>·6H<sub>2</sub>O was dissolved in 28 mL of ethylene glycol (EG) by 15 min ultrasonic vibration to make FeCl<sub>3</sub>·6H<sub>2</sub>O completely dissolve. Then, 2.4 g of anhydrous sodium acetate and 0.2 g of polyethylene glycol (PEG) were added to the FeCl<sub>3</sub> solution and stirred for 30 min. Ultrasound was performed for 15 min after stirring PEG for 30 min, for PEG was difficult to dissolve. Finally, the mixed solution was transferred to a 50 mL high-pressure reactor and continuously heated to 200 °C in an electric blast-drying oven for 8 h. Then, the blast-drying oven was turned off and the solution was cooled at room temperature naturally. The Fe<sub>3</sub>O<sub>4</sub> solution was poured into a beaker to separate the Fe<sub>3</sub>O<sub>4</sub> nanoparticles by a magnet and the supernatant was removed. Then, Fe<sub>3</sub>O<sub>4</sub> nanoparticles were washed with ultrapure water and anhydrous ethanol, alternately, 3 times, and were dried at 60 °C for 6 h in an electric blast-drying oven [1,18,19].

#### 2.2.2. Synthesis of Fe<sub>3</sub>O<sub>4</sub>@PDA

First, 2 mg dopamine was added to 6 mL Tris-HCl buffer solution (pH = 8.4) and ultrasound to obtain a uniform PDA@Tris-HCl dispersion. Next, 40 mg Fe<sub>3</sub>O<sub>4</sub> nanoparticles were added to the solution under constant ultrasound until they were completely dissolved in the PDA/Tris-HCl solution, and, then, after magnetic stirring for 3 h, Fe<sub>3</sub>O<sub>4</sub>@PDA

products were separated from the solution by an external magnetic field. Lastly, the as-obtained products were washed with ultrapure water three times and dried at 50 °C for 12 h to yield Fe<sub>3</sub>O<sub>4</sub>@PDA [20].

### 2.2.3. Synthesis of Fe<sub>3</sub>O<sub>4</sub>@PDA@Ag

First, 10 mg Fe<sub>3</sub>O<sub>4</sub>@PDA was added to 20 mL ultrapure water to obtain a uniform dispersion under ultrasound. Next, 100 mL 0.001 mol/L AgNO<sub>3</sub> solution was poured gently into the solution mentioned above with constant stirring and heating [19]. When the solution temperature reached 90 °C, 0.0258 g sodium citrate solution was added, and the reaction took 1.5 h. Fe<sub>3</sub>O<sub>4</sub>@PDA@Ag products were separated from the solution by an external magnetic field. Eventually, the as-obtained products were washed with ultrapure water 3 times and dried at 50 °C for 12 h to yield Fe<sub>3</sub>O<sub>4</sub>@PDA@Ag [16].

### 2.2.4. Synthesis of Fe<sub>3</sub>O<sub>4</sub>@PDA@Ag@GO

First, 10 mg of Fe<sub>3</sub>O<sub>4</sub>@PDA@Ag was dissolved in water, 0.5 mL 0.5 mol/L of GO dispersion was added, and ultrapure water was added to make the volume of solution 12 mL with magnetic stirring for 3 h. Next, the as-obtained products were washed with ultrapure water 3 times [20], and Fe<sub>3</sub>O<sub>4</sub>@PDA@Ag@GO products were separated from the solution by an external magnetic field. At last, ultrapure water was added to make the volume of solution 10 mL [16].

## 3. Results and Discussion

### 3.1. Characterization

#### 3.1.1. UV-Visible Characterization

The UV-vis spectra in Figure 1 illustrate the maximum absorption of Ag NPs synthesized by various reaction temperatures, which are located at the range of 300–700 nm to study the effect of reaction temperature on the preparation of silver sol. The reaction temperatures were 70 °C, 80 °C, 90 °C and 100 °C, respectively.

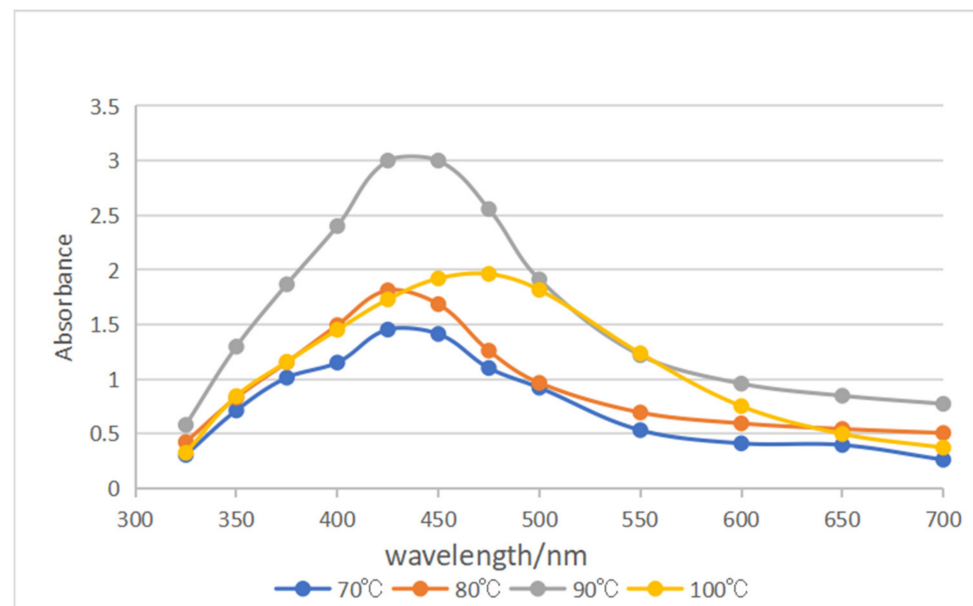


**Figure 1.** UV absorption spectra of silver dissolved at different temperatures.

The prepared AgNO<sub>3</sub> solution (0.001 mol/L, 100 mL) were added to four beakers, respectively, and 0.0258 g sodium citrate were added to each of the four beakers and were heated, respectively, to 70 °C, 80 °C, 90 °C and 100 °C for 1.5 h.

It was observed that the color of the solution heated to 70 °C was lighter than others, and precipitation occurred in the solution that was heated to 100 °C. It is shown in Figure 1 that the strongest absorption peaks of the four beakers of silver sol were located between 400–500 nm, and the strongest absorption peak for each of the silver sol was located at 425 nm when the solution was heated to 70 °C, 80 °C and 90 °C. When the silver sol was heated to 70 °C, the concentration was low for the reaction was incomplete. When the temperature was as high as 100 °C, the strongest absorption peak moved to right and the concentration was also low for the aggregate sank to the bottom. The preparation of Ag NPs followed the procedure reported in the literature [37,38]. Therefore, the most suitable heating temperature for synthesizing Fe<sub>3</sub>O<sub>4</sub>@PDA@Ag is 90 °C.

### 3.1.2. TEM Image of Fe<sub>3</sub>O<sub>4</sub>@PDA@Ag@GO

The size, morphology and surface composition of Fe<sub>3</sub>O<sub>4</sub>@PDA@Ag@GO were characterized by TEM (FEI Talos F200×, FEI Company, Hillsborough, OR, USA) [16].

As is shown in Figures 2 and 3, most nanoparticles are spherical, with magnifications of 1 μm, 500 nm, 200 nm and 100 nm, respectively. AgNPs are evenly distributed on the GO surface without large aggregate generation, which indicates that Ag NPs can be adsorbed effectively on the GO surface and GO plays a good role in dispersing Ag NPs.

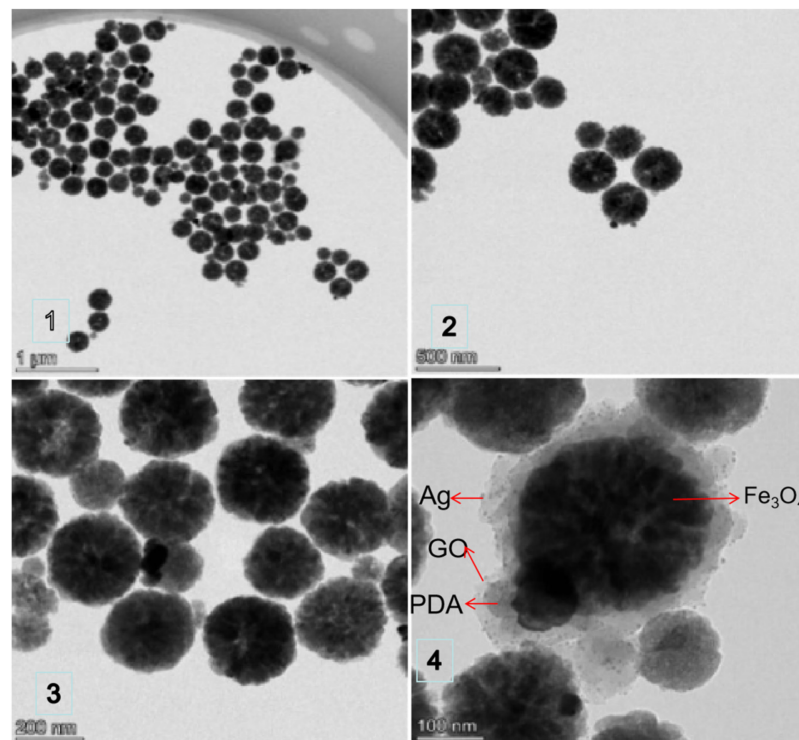


**Figure 2.** TEM images Fe<sub>3</sub>O<sub>4</sub>@PDA@Ag@GO of different magnifications. (1) TEM image zoomed to 1 μm; (2) TEM image zoomed to 500 nm; (3) TEM image zoomed to 200 nm; (4) TEM image zoomed to 100 nm.

When zoomed to 100 nm, as is shown in the following pictures, Fe<sub>3</sub>O<sub>4</sub> is clustered in the innermost layer. The interlayer between globular Fe<sub>3</sub>O<sub>4</sub> and Ag nanoparticles is PDA, the black dots are Ag nanoparticles and the outermost layer is GO.

The peaks of Ag, Fe, C and O can be obtained by EDS analysis of Fe<sub>3</sub>O<sub>4</sub>@PDA@Ag@GO nanocomposite in (6) in the Figure 3, which proves that there are Ag, Fe, C and O in the substrate and Fe<sub>3</sub>O<sub>4</sub>@PDA@Ag@GO was successfully synthesized [21].

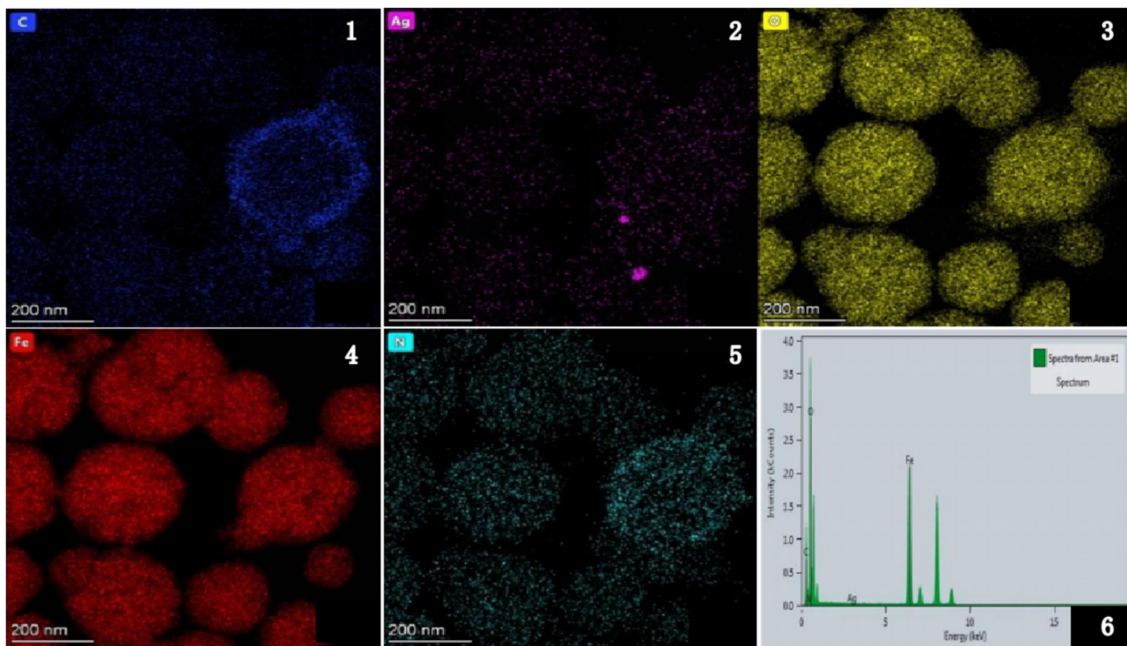


**Figure 3.** TEM mapping and EDS of  $\text{Fe}_3\text{O}_4@\text{PDA}@\text{Ag}@\text{GO}$  nanocomposites. (1) The elemental mappings of C; (2) the elemental mappings of Ag; (3) the elemental mappings of O; (4) the elemental mappings of Fe; (5) the elemental mappings of N; (6) EDS of  $\text{Fe}_3\text{O}_4@\text{PDA}@\text{Ag}@\text{GO}$ .

### 3.1.3. XRD Characterization

The crystal phase was characterized by D8-Advance X-ray diffraction (XRD, Bruker, Germany, Copper  $\text{K}\alpha$  radiation). The range of the scanning angle was  $(5\text{--}85)^\circ$  and the scanning rate was  $8^\circ/\text{min}$  [20].

Figure 4 shows the XRD patterns of  $\text{Fe}_3\text{O}_4@\text{PDA}@\text{Ag}@\text{GO}$ . The corresponding peaks of  $\text{Fe}_3\text{O}_4$  crystal occurred at  $30^\circ$ ,  $35^\circ$ ,  $43^\circ$ ,  $57^\circ$  and  $62^\circ$ . The peaks corresponding to silver crystals were at  $38^\circ$ ,  $44^\circ$ ,  $64^\circ$  and  $77^\circ$ , which were consistent with the peaks in the literature. According to the XRD analysis above, there were  $\text{Fe}_3\text{O}_4$  nanoparticles and Ag nanoparticles in SERS substrate [22].

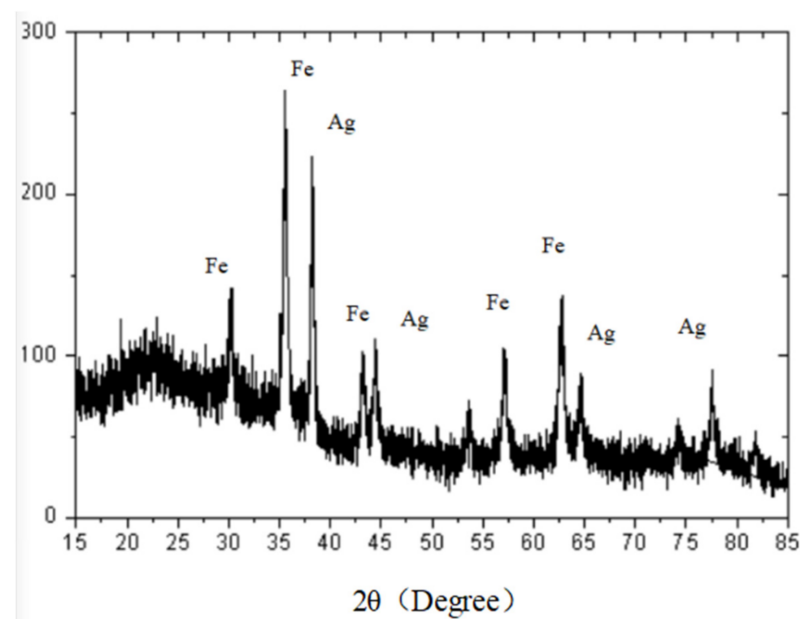


**Figure 4.** XRD of  $\text{Fe}_3\text{O}_4@\text{PDA}@\text{Ag}@\text{GO}$ .

### 3.2. Detection of PAHs with SERS Substrate

#### 3.2.1. Sample Preparation

First, 0.1 g of PAHs were added to a moderate amount of alcohol under ultrasound for 30 min and then magnetically stirred for 2 h. Next, the as-prepared solution was poured into a 100 mL volumetric bottle with constant volume to prepare a PAHs methanol solution with a concentration of 1 g/L. Finally, PAHs solutions of different concentrations were prepared by diluting 1 g/L of PAH methanol solution with methanol and ultrapure water [16].

#### 3.2.2. Method for Detection

Raman spectroscopy was performed on a Metage Opal 2800 Raman spectrometer with an excitation wavelength of 785 nm. First, the portable spectrometer was turned on and preheated for 30 min in order to check whether the instrument and laser work properly. Next, the PAHs solution and the prepared  $\text{Fe}_3\text{O}_4@\text{PDA}@Ag@\text{GO}$  substrate were added to a brown sample bottle in proportion. The integral time was set for 15~30 s, and the laser intensity was set at 90. Then, the average value of each sample was shown after the value of the sample was recorded 4 times. Finally, the Raman spectrum was obtained when the background was subtracted, and the dark current was deducted.

#### 3.2.3. The Detection of Phenanthrene

Figure 5 illustrates the influences of the synthesis of  $\text{Fe}_3\text{O}_4@\text{PDA}@Ag@\text{GO}$  material on the Raman enhancement of PAHs solution. Phenanthrene solid,  $10^{-2}$  g/L phenanthrene solution, the mixture of  $10^{-2}$  g/L phenanthrene solution and SERS substrate and  $\text{Fe}_3\text{O}_4@\text{PDA}@Ag@\text{GO}$  solution were detected. The detection results are displayed in Figure 5.

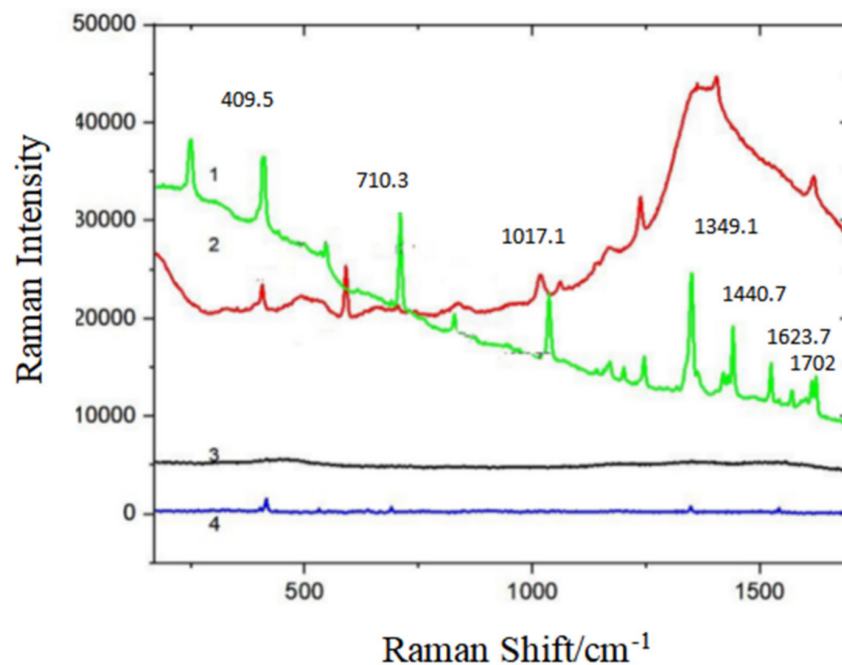


**Figure 5.** SERS spectra of phenanthrene (1) phenanthrene solid; (2) the mixture of  $10^{-2}$  g/L phenanthrene and SERS substrate solution; (3)  $\text{Fe}_3\text{O}_4@\text{PDA}@Ag@\text{GO}$  solution; (4)  $10^{-2}$  g/L phenanthrene solution.

PAHs can be differentiated based upon their characteristic SERS peaks [39]. The  $10^{-2}$  g/L phenanthrene solution ((4) in the Figure 5) has a characteristic peak with a low intensity, while the characteristic peak of  $\text{Fe}_3\text{O}_4@\text{PDA}@Ag@\text{GO}$  substrate ((3) in the Figure 5) is negligible. When  $10^{-2}$  g/L phenanthrene solution is mixed with  $\text{Fe}_3\text{O}_4@\text{PDA}@Ag@\text{GO}$  substrate, an obvious Raman characteristic peak ((2) in the Figure 5) appears, which is located at  $402.7\text{ cm}^{-1}$ ,

1017.12  $\text{cm}^{-1}$ , 1238.64  $\text{cm}^{-1}$ , 1405.63  $\text{cm}^{-1}$  and 1614.98  $\text{cm}^{-1}$  that corresponds to the peak of phenethene solid ((1) in the Figure 5). The results show that  $\text{Fe}_3\text{O}_4@\text{PDA}@Ag@\text{GO}$  substrate enhances the adsorption capacity of  $10^{-2}$  g/L phenanthrene standard solution, and the Raman effect on the surface phenanthrene is obviously enhanced.

### 1. Effects of each component in $\text{Fe}_3\text{O}_4@\text{PDA}@Ag@\text{GO}$ on SERS detection performance

It is illustrated by (3) in the Figure 6 and (4) in the Figure 6 that the characteristic peak is negligible.  $\text{Fe}_3\text{O}_4$  and  $\text{Fe}_3\text{O}_4@\text{PDA}$  do not enhance the SERS activity of the phenanthrene solution of  $10^{-2}$  g/L. This may result from the fact that PDA covered  $\text{Fe}_3\text{O}_4$ , thus the SERS activity of  $\text{Fe}_3\text{O}_4$  not being shown. It is illustrated by (1) in the Figure 6 and (2) in the Figure 6 that  $\text{Fe}_3\text{O}_4@\text{PDA}@Ag@\text{GO}$  has a stronger Raman signal than  $\text{Fe}_3\text{O}_4@\text{PDA}@Ag$ .  $\text{Fe}_3\text{O}_4@\text{PDA}@Ag@\text{GO}$  substrate has a combined enhancement of the electromagnetic enhancement of Ag and the chemical enhancement of GO. The adsorption capacity of the phenanthrene standard solution of  $10^{-2}$  g/L is increased and the sensitivity is improved.

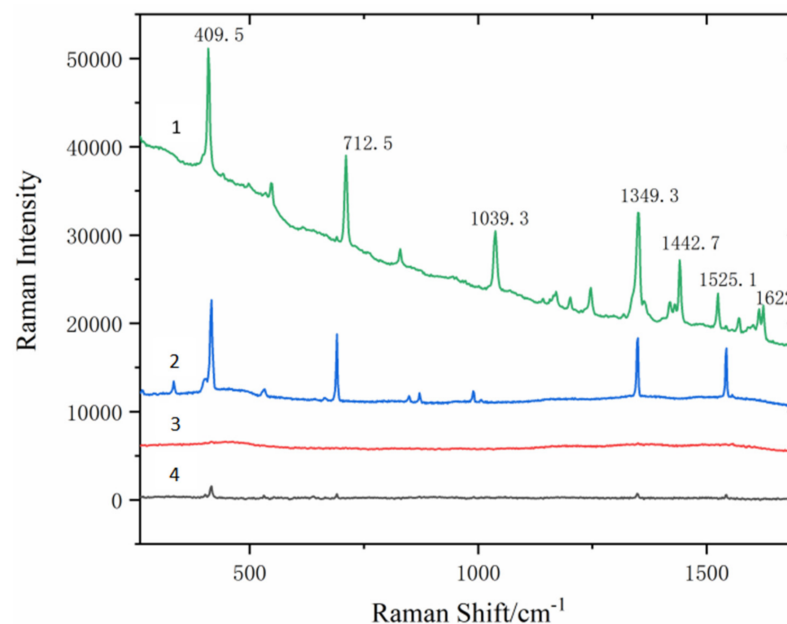


**Figure 6.** SERS signal of phenanthrene captured on  $\text{Fe}_3\text{O}_4@\text{PDA}@Ag@\text{GO}$ ,  $\text{Fe}_3\text{O}_4@\text{PDA}@Ag$ ,  $\text{Fe}_3\text{O}_4@\text{PDA}$  and  $\text{Fe}_3\text{O}_4$ , respectively (1)  $\text{Fe}_3\text{O}_4@\text{PDA}@Ag@\text{GO}$  substrate; (2)  $\text{Fe}_3\text{O}_4@\text{PDA}@Ag$  substrate; (3)  $\text{Fe}_3\text{O}_4@\text{PDA}$  substrate; (4)  $\text{Fe}_3\text{O}_4$  substrate.

### 2. The influence of the mixing ratio of SERS substrate and phenanthrene solution on SERS detection performance

In the experiment, the ratio of the mixture of the substrate and the solution also affected the value of Raman spectral peak. The volume ratio of the substrate and the solution was studied to find the optimal ratio. The mixed solutions of the different volume ratio of 2:1, 1:1, 1:2 and 1:4 were used to study the influence of the volume ratio of the mixture of SERS substrate with phenanthrene solution on SERS detection performance.

As shown in Figure 7, Raman spectral peaks of the mixed solution of the substrate and the phenanthrene solution change with their different volume ratios. Raman characteristic peaks are located at 590.7  $\text{cm}^{-1}$ , 1037.3  $\text{cm}^{-1}$ , 1238.6  $\text{cm}^{-1}$ , 1530.5  $\text{cm}^{-1}$  and 1614.9  $\text{cm}^{-1}$ . The Raman displacement of the Raman spectral peak of the solution has shifted, possibly due to fluorescence interference. The peak heights of the spectrum from 1 to 4 are 2570.4, 3157.2, 4293.7 and 2904.6, respectively. Therefore, the volume ratio corresponding to spectrum 3 is chosen for the optimal ratio to be ready for the next step of the experiment.

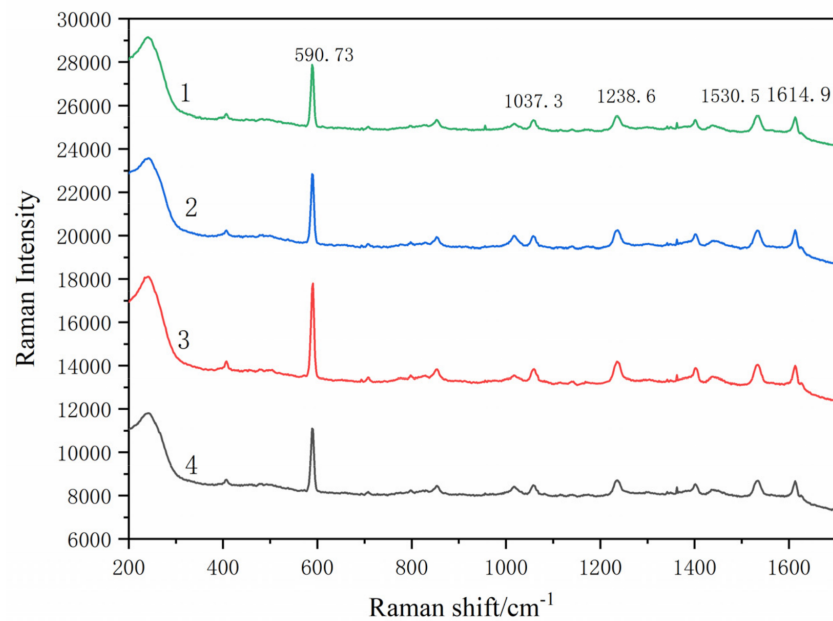


**Figure 7.** SERS spectra of different mixing volume ratios of  $\text{Fe}_3\text{O}_4@\text{PDA}@\text{Ag}@\text{GO}$  substrate and phenanthrene solution (1) 2:1;(2) 1:1; (3) 1:2; (4) 1:4.

Raman spectral intensity is the strongest when the volume ratio of substrate to standard solution is 1:2. The intensity of Raman spectrum peak reduces as the amount of substrate decreases. The number of molecules in hot spots on SERS substrate increases with the increase in the amount of the substrate. Therefore, the Raman intensity is intensified significantly. However, when the concentration of the substrate increases to a certain value and the enriched phenanthrene solution reaches the limit, the substrate interferes with the Raman signal, thus decreasing the spectral intensity.

### 3. $\text{Fe}_3\text{O}_4@\text{PDA}@\text{Ag}@\text{GO}$ detection limit for phenanthrene

In order to explore the influence of the synthesis of  $\text{Fe}_3\text{O}_4@\text{PDA}@\text{Ag}@\text{GO}$  material on the Raman enhancement of phenanthrene solution and to detect the detection limit of phenanthrene, the phenanthrene solution at different concentrations from  $10^{-5}$  g/L to  $10^{-8}$  g/L is mixed with the substrate of  $\text{Fe}_3\text{O}_4@\text{PDA}@\text{Ag}@\text{GO}$  and the Raman spectra is captured as shown in Figure 8.

As shown in Figure 8, the intensity of characteristic peak of the mixture of the phenanthrene solution ( $10^{-5}\sim 10^{-8}$  g/L) and the substrate decreases as the concentration of the solution is decreased. When the concentration of the phenanthrene solution reaches  $10^{-8}$  g/L, a slight characteristic peak can still be seen, thus demonstrating that the detection limit of  $\text{Fe}_3\text{O}_4@\text{PDA}@\text{Ag}@\text{GO}$  for phenanthrene solution can reach  $10^{-8}$  g/L.

In order to study the linear relationship between the intensities of characteristic peaks and the logarithm of phenanthrene concentration, two characteristic peaks of phenanthrene,  $411\text{ cm}^{-1}$  and  $590\text{ cm}^{-1}$ , were analyzed which was shown in Figure 9.

The SERS peak intensities versus the logarithm of phenanthrene concentration had a good linear relationship from  $10^{-8}$  to  $10^{-5}$  g/L (Figure 9). The calibration equation can be described as (the characteristic absorption peaks located at  $411\text{ cm}^{-1}$ )  $y_1 = 9415.1089x + 456.1223$ . The linear regression equation (the characteristic absorption peaks located at  $590\text{ cm}^{-1}$ ) is  $y_2 = 11,736.837x + 1092.2970$ . The error bars indicate that the standard is derived from a total of 10 measurements. The present results reveal the potential for this method to be a rapid analysis and detection of phenanthrene at low concentrations.

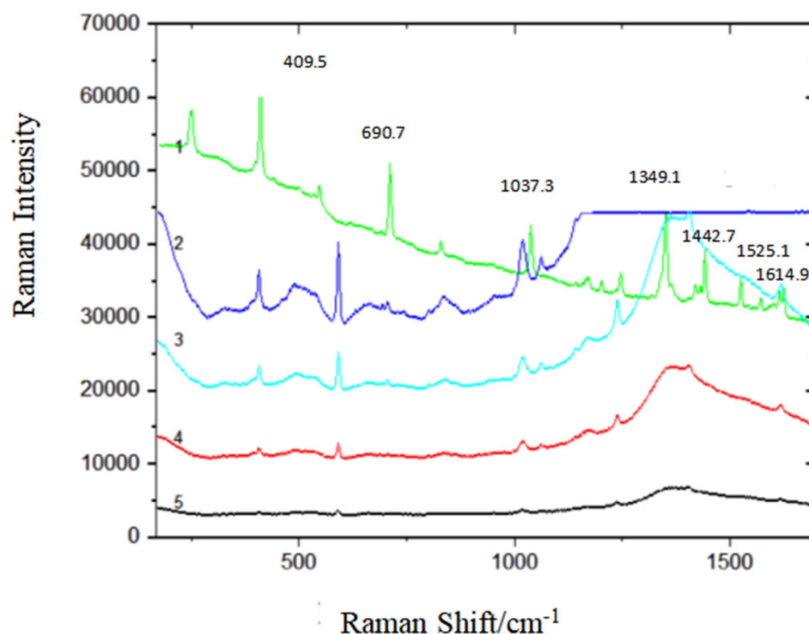


**Figure 8.** The detection limit of phenanthrene captured on Fe<sub>3</sub>O<sub>4</sub>@PDA@Ag@GO nanocomposites SERS substrate (1) phenanthrene solid; (2) 10<sup>-5</sup> g/L phenanthrene SERS solution; (3) 10<sup>-6</sup> g/L phenanthrene SERS solution; (4) 10<sup>-7</sup> g/L phenanthrene SERS solution; (5) 10<sup>-8</sup> g/L phenanthrene SERS solution.

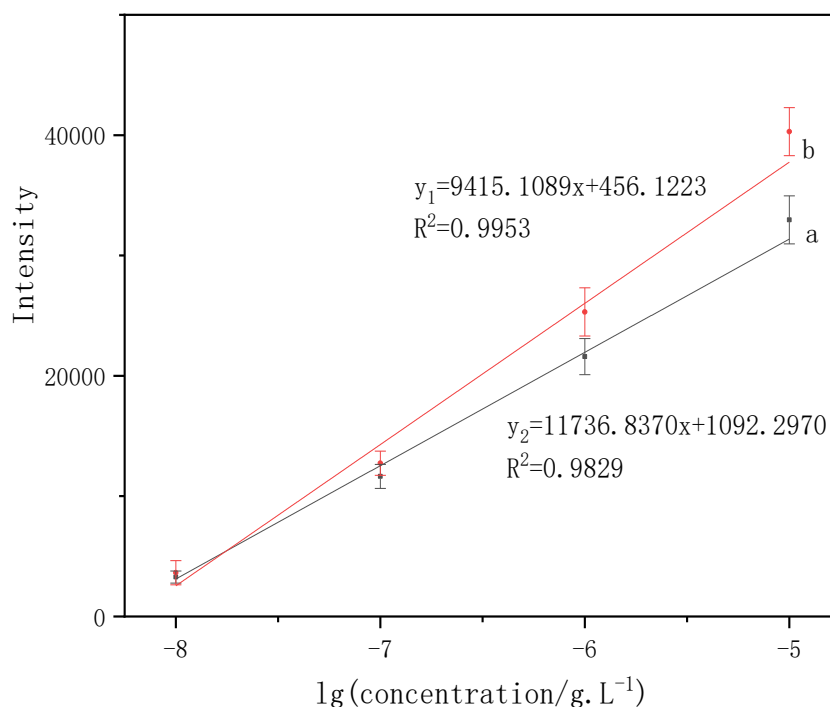


**Figure 9.** Linear relationships between the phenanthrene characteristic intensity and the logarithm of phenanthrene concentration. (a) 590 cm<sup>-1</sup>; (b) 411 cm<sup>-1</sup>.

3.2.4. Limit of Detection for Pyrene

In order to explore the influence of the synthesis of Fe<sub>3</sub>O<sub>4</sub>@PDA@Ag@GO material on the Raman enhancement of pyrene standard solution and to detect the detection limit of pyrene, the pyrene solution at different concentrations from 10<sup>-5</sup> g/L to 10<sup>-8</sup> g/L is mixed

with the substrate of Fe<sub>3</sub>O<sub>4</sub>@PDA@Ag@GO and the Raman spectra is captured as shown in Figure 10.

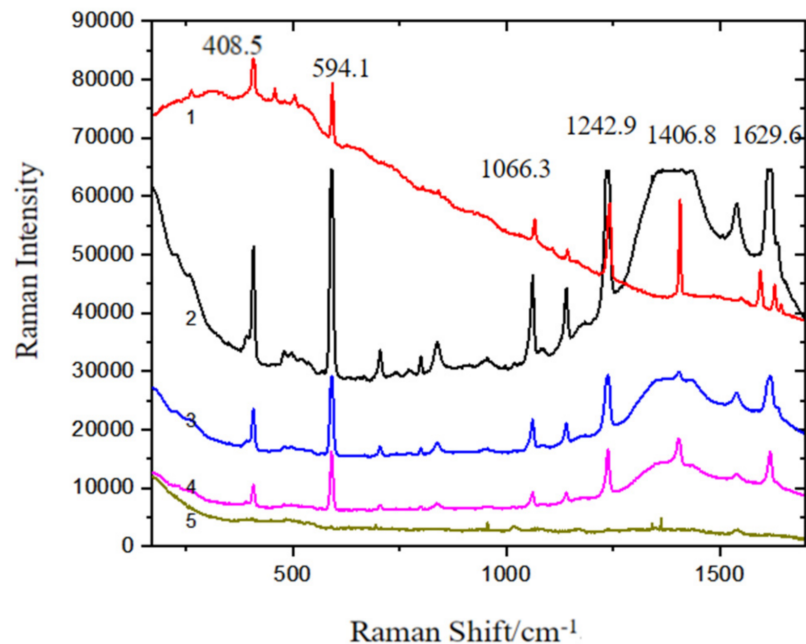


**Figure 10.** The detection limit of Pyrene captured on Fe<sub>3</sub>O<sub>4</sub>@PDA@Ag@GO nanocomposites SERS substrate (1) Pyrene solid; (2) 10<sup>-5</sup> g/L Pyrene SERS solution; (3) 10<sup>-6</sup> g/L Pyrene SERS solution; (4) 10<sup>-7</sup> g/L Pyrene SERS solution; (5) 10<sup>-8</sup> g/L Pyrene SERS solution.

As shown in Figure 10, the intensity of the characteristic peak of the mixture blending the pyrene standard solution (10<sup>-5</sup>~10<sup>-8</sup> g/L) with the substrate decreases with the decrease of the concentration of the solution. When the concentration of the pyrene standard solution reaches 10<sup>-7</sup> g/L, the spectral signal is apparent, and the characteristic peak is clearly visible. However, when the concentration reaches 10<sup>-8</sup> g/L, the spectral signal disappears and almost becomes a straight line. Therefore, the detection limit of Fe<sub>3</sub>O<sub>4</sub>@PDA@Ag@GO for pyrene solution is 10<sup>-7</sup> g/L.

In order to study the linear relationship between the intensities of characteristic peaks and the logarithm of pyrene concentration, two characteristic peaks of pyrene, 590 cm<sup>-1</sup> and 1016 cm<sup>-1</sup>, were analyzed which was shown in Figure 11.

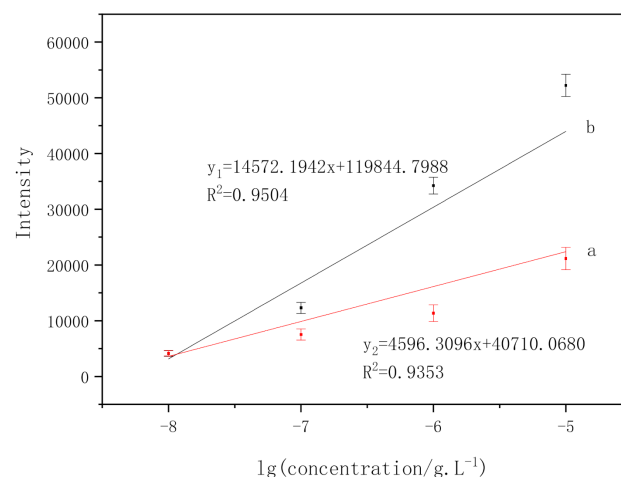


**Figure 11.** Linear relationships between the pyrene characteristic intensity and the logarithm of pyrene concentration. (a) 1016 cm<sup>-1</sup>; (b) 590 cm<sup>-1</sup>.

The SERS peak intensities versus the logarithm of pyrene concentration had a good linear relationship from  $10^{-8}$  g/L to  $10^{-5}$  g/L (Figure 12). The calibration equation can be described as (the characteristic absorption peaks located at  $590\text{ cm}^{-1}$ )  $y_1 = 14,572.1942x + 119,844.7988$ . The linear regression equation (the characteristic absorption peak is located at  $1016\text{ cm}^{-1}$ ) is  $y_2 = 4596.3096x + 40,710.068$ . The error bars indicate that the standard is derived from a total of 10 measurements. The present results reveal the potential of this method to do rapid analysis and detection of pyrene at low concentrations.

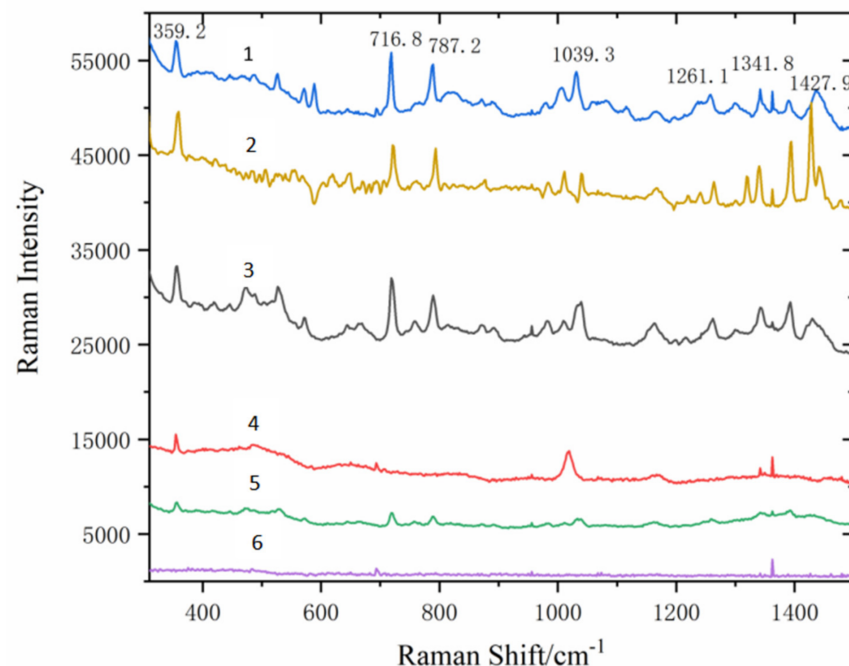


**Figure 12.** The detection limit of benzantracene captured on  $\text{Fe}_3\text{O}_4@\text{PDA}@\text{Ag}@\text{GO}$  nanocomposites SERS substrate (1)  $10^{-4}$  g/L benzantracene standard solution; (2) benzantracene solid; (3)  $10^{-5}$  g/L benzantracene standard solution; (4)  $10^{-6}$  g/L benzantracene standard solution; (5)  $10^{-7}$  g/L benzantracene standard solution; (6)  $10^{-8}$  g/L benzantracene standard solution.

### 3.2.5. Detection Limit of Benzantracene

In order to explore the influence of the synthesis of  $\text{Fe}_3\text{O}_4@\text{PDA}@\text{Ag}@\text{GO}$  material on the Raman enhancement of benzantracene solution and to detect the detection limit of benzantracene, the benzantracene solution at different concentrations from  $10^{-5}$  g/L to  $10^{-8}$  g/L is mixed with the substrate of  $\text{Fe}_3\text{O}_4@\text{PDA}@\text{Ag}@\text{GO}$  and the Raman spectra is captured as shown in Figure 12.

As shown in Figure 12, the intensity of the characteristic peak of the mixture blending the benzantracene solution ( $10^{-5}\sim 10^{-8}$  g/L) with the substrate decreases with the decrease of the concentration of the solution. When the concentration of the benzantracene solution reaches  $10^{-7}$  g/L, the spectral signal almost disappears, but a weak characteristic peak can still be seen. However, when the concentration reaches  $10^{-8}$  g/L, the spectral signal disappears and almost becomes a straight line. Therefore, the detection limit of  $\text{Fe}_3\text{O}_4@\text{PDA}@\text{Ag}@\text{GO}$  for benzantracene solution is  $10^{-7}$  g/L.

In order to study the linear relationship between the intensities of characteristic peaks and the logarithm of benzantracene concentration, two characteristic peaks of benzantracene located at  $356\text{ cm}^{-1}$  and  $1033\text{ cm}^{-1}$  were analyzed as shown in Figure 13.

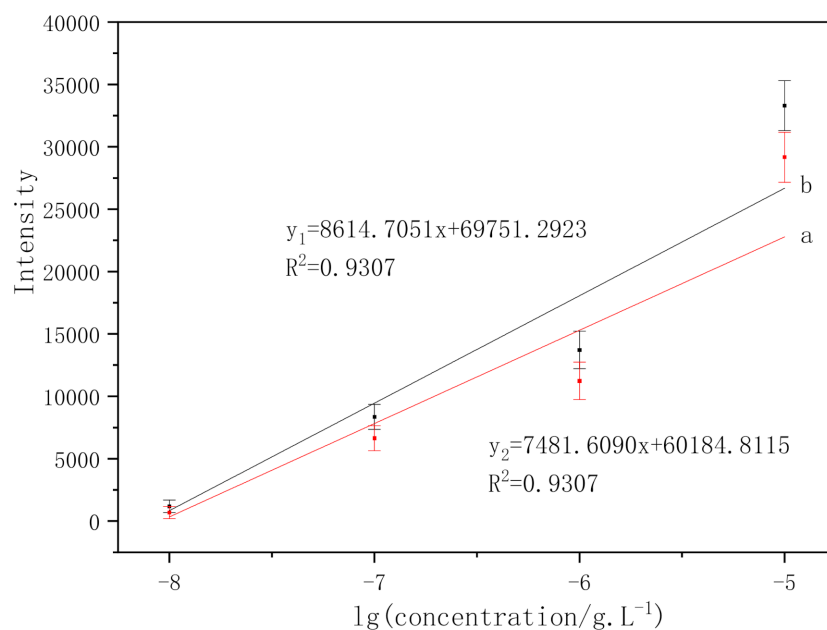


**Figure 13.** Linear relationships between the benzoanthracene characteristic intensity and the logarithm of benzoanthracene concentration. (a) 1033  $\text{cm}^{-1}$ ; (b) 356  $\text{cm}^{-1}$ .

The linear relationships between the SERS intensity and the logarithm of benzoanthracene concentrations (from  $10^{-8}$  g/L to  $10^{-5}$  g/L) are detected in Figure 13. The intensity of the characteristic peak decreases with the decrease of concentration. The fitting linear relationship in line a (the characteristic absorption peaks located at 1033  $\text{cm}^{-1}$ ) of Figure 13 is  $y_2 = 7481.609x + 60,184.8115$  while that in line b (the characteristic absorption peaks located at 356  $\text{cm}^{-1}$ ) of Figure 13 is  $y_1 = 8614.7051x + 69,751.2923$ . The x is the logarithm of solution concentration and the y is the relative intensity.

#### 4. Conclusions

$\text{Fe}_3\text{O}_4@\text{PDA}@\text{Ag}@\text{GO}$  substrate with high SERS activity was prepared and its morphology and structure were characterized in the experiment. By investigating the effects of different heating temperatures on the preparation of silver sol, it is discovered that the concentration of AgNPs is the highest when heated to 90 °C and the SERS signal intensity of surface polycyclic aromatic hydrocarbons (PAHs) is the highest. The study on the influence of different components of composite substrate on SERS also observes that Ag and GO enhanced the Raman signal in the  $\text{Fe}_3\text{O}_4@\text{PDA}@\text{Ag}@\text{GO}$  substrate [16]; the detection limit of phenanthrene is  $10^{-8}$  g/L, that of pyrene  $10^{-7}$  g/L and that of benzoanthracene  $10^{-7}$  g/L, when  $\text{Fe}_3\text{O}_4@\text{PDA}@\text{Ag}@\text{GO}$  is used as SERS substrate. The composite nanoparticles have good magnetic response, can separate quickly and enrich the molecules to be measured and shorten the pretreatment time [16]. Therefore,  $\text{Fe}_3\text{O}_4@\text{PDA}@\text{Ag}@\text{GO}$  can be used as SERS substrate for the enrichment and detection of trace PAHs in the environment [23].

**Author Contributions:** The first author J.L. conceptualized the experiments and wrote the manuscript, and submitted it for publication.; J.W. performed experiments, data curation, and the design methodology.; Y.W. performed analysis and participated in technical discussion.; L.G. and K.G. performed visualization and supervision.; W.C. performed review and editing.; S.S. performed principal investigator (PI) of the research and organized the data, All authors have read and agreed to the published version of the manuscript.

**Funding:** This research was supported by the Science and technology research project of Chongqing Education Commission in China (No. KJQN202012907), Natural Science Foundation of Chongqing in China (No. cstc2020jcyj-msxmX0274).

**Data Availability Statement:** The data presented in this study are available on request from the corresponding author.

**Conflicts of Interest:** The authors declare no conflict of interest.

## References

1. Wang, X.; Hao, W.; Zhang, H.; Pan, Y.; Kang, Y.; Zhang, X.; Zou, M.; Tong, P.; Du, Y. Analysis of polycyclic aromatic hydrocarbons in water with gold nanoparticles decorated hydrophobic porous polymer as surface-enhanced Raman spectroscopy substrate. *Spectrochim. Acta Part A Mol. Biomol. Spectrosc.* **2015**, *139*, 214–221. [[CrossRef](#)] [[PubMed](#)]
2. Chen, H.; Xia, D.; Yuan, Y. Surface Enhanced Raman Spectroscopic Investigation of PAHs at a PDMS-Au Composite Substrate PDMS-Au. *Chem. Res.* **2017**, *38*, 376–382.
3. Wang, M.; Zhang, S.; Wang, C. Assessment of gaseous phase PAHs emitted from marine diesel engine using vortex-assisted dispersive liquid-liquid microextraction followed by GC/MS. In *First International Conference on Information Sciences, Machinery, Materials and Energy*; Atlantis Press: Amsterdam, The Netherlands, 2015; pp. 1841–1846. [[CrossRef](#)]
4. Rota, M.; Bosetti, C.; Boccia, S.; Boffetta, P.; la Vecchia, C. Occupational expo-cancers: an updated systematic review and a meta-analysis to 2014. *Arch. Toxicol.* **2014**, *88*, 1479–1490. [[CrossRef](#)] [[PubMed](#)]
5. White, A.J.; Bradshaw, P.T.; Herring, A.H.; Teitelbaum, S.L.; Beyea, J.; Stellman, S.D.; Steck, S.E.; Mordukhovich, I.; Eng, S.M.; Engel, L.S.; et al. Exposure to multiple sources of polycyclic aromatic hydrocarbons and breast cancer incidence. *Environ. Int.* **2016**, *89–90*, 185–192. [[CrossRef](#)]
6. Nsiband, S.A.; Montaseri, H.; Forbes, P.B.C. Advances in the application of nanomaterial-based sensors for detection of polycyclic aromatic hydrocarbons in aquatic systems. *Trends Anal. Chem.* **2019**, *115*, 52–69. [[CrossRef](#)]
7. Marzooghi, S.; di Toro, D.M. A critical review of polycyclic aromatic hydrocarbon phototoxicity models. *Environ. Toxicol. Chem.* **2017**, *36*, 1138–1148. [[CrossRef](#)]
8. Ni, Y.; Wang, P.; Song, H.; Lin, X.; Kokot, S. Electrochemical detection of benzo(a)pyrene and related DNA damage using DNA/hemin/nafion-graphene biosensor. *Anal. Chim. Acta* **2014**, *821*, 34–40. [[CrossRef](#)]
9. De Paepe, E.; Wauters, J.; Van Der Borgh, M.; Claes, J.; Huysman, S.; Croubels, S.; Vanhaecke, L. Ultra-high-performance liquid chromatography coupled to quadrupole orbitrap high-resolution mass spectrometry for multi-residue screening of pesticides, (veterinary) drugs and mycotoxins in edible insects. *Food Chem.* **2019**, *293*, 187–196. [[CrossRef](#)]
10. Martakidis, K.; Gavril, D. New inverse gas chromatographic methodology for studying mass transfer caused by the evaporation of volatile liquids. *Instrum. Sci. Technol.* **2019**, *47*, 389–409. [[CrossRef](#)]
11. Rama, M.J.R.; Ruiz-Medina, A.; Díaz, A.M. A Simple and Straightforward Procedure for Monitoring Phenol Compounds in Waters by Using UV Solid Phase Transduction Integrated in a Continuous Flow System. *Mikrochim. Acta* **2003**, *141*, 143–148. [[CrossRef](#)]
12. Matthew, B.; Paolo, B.; Mariangela, C. Analysis of poly-cyclic aromatic hydrocarbons (PAHs) in airborne particles by direct sample introduction thermal desorption GC / MS. *Atmos. Environ.* **2008**, *42*, 6144–6151.
13. Chen, Y.; Liu, H.; Tian, Y.; Du, Y.; Ma, Y.; Zeng, S.; Gu, C.; Jiang, T.; Zhou, J. In situ recyclable surface-enhanced Raman scattering-based detection of multicomponent pesticide residues on fruits and vegetables by the flower-like MoS<sub>2</sub>@Ag hybrid substrate. *ACS. Appl. Mater. Inter.* **2020**, *12*, 14386–14399. [[CrossRef](#)]
14. Du, Y.; Liu, H.; Chen, Y.; Tian, Y.; Zhang, X.; Gu, C.; Jiang, T.; Zhou, J. Recyclable label-free SERS-based immunoassay of PSA in human serum mediated by enhanced photocatalysis arising from Ag nanoparticles and external magnetic field. *Appl. Surf. Sci.* **2020**, *528*, 146953. [[CrossRef](#)]
15. Kalachyova, Y.; Mares, D.; Jerabek, V.; Elashnikov, R.; Švorčík, V.; Lyutakov, O. Longtime stability of silver-based SERS substrate in the environment and (bio)environment with variable temperature and humidity. *Sens. Actuators A Phys.* **2018**, *285*, 566–572. [[CrossRef](#)]
16. Botta, R.; Eiamchai, P.; Horprathum, M.; Limwichean, S.; Chananonawathorn, C.; Patthanasettakul, V.; Maezono, R.; Jomphoak, A.; Nuntawong, N. 3D structured laser engraves decorated with gold nanoparticle SERS chips for paraquat herbicide detection in environments. *Sens. Actuators B Chem.* **2019**, *304*, 127327. [[CrossRef](#)]
17. Zhou, Y.; Liang, P.; Zhang, D.; Tang, L.; Dong, Q.; Jin, S.; Ni, D.; Yu, Z.; Ye, J. A facile seed growth method to prepare stable Ag@ZrO<sub>2</sub> core-shell SERS substrate with high stability in extreme environments. *Spectrochim. Acta Part A Mol. Biomol. Spectrosc.* **2020**, *228*, 117676. [[CrossRef](#)]
18. Liu, J.; Liu, Y.; Cao, Y.; Sang, S.; Guan, L.; Wang, Y.; Wang, J. Preparation of FeO@PDA@Au@GO Composite as SERS Substrate and Its Application in the Enrichment and Detection for Phenanthrene. *Micromachines* **2022**, *1*, 128. [[CrossRef](#)]
19. Liu, K.; Bai, Y.; Zhang, L.; Yang, Z.; Fan, Q.; Zheng, H.; Yin, Y.; Gao, C. Porous Au–Ag Nanospheres with High-Density and Highly Accessible Hotspots for SERS Analysis. *Nano Lett.* **2016**, *16*, 3675–3681. [[CrossRef](#)]
20. Yi, Z.; Niu, G.; Luo, J.; Kang, X.; Yao, W.; Zhang, W.; Yi, Y.; Yi, Y.; Ye, X.; Duan, T.; et al. Ordered array of Ag semishells on different diameter monolayer polystyrene colloidal crystals: An ultrasensitive and reproducible SERS substrate. *Sci. Rep.* **2016**, *6*, 32314. [[CrossRef](#)]
21. Zhu, T.; Sun, Y.; Lu, W.; Wang, G.; Zhang, X.; Chen, S.; Zhang, C.; Li, Z.; Man, B.; Yang, C. Theoretical and experimental investigation of the flexible Ag nano-tree@Cu mesh SERS substrate. *J. Alloys Compd.* **2022**, *908*, 164622. [[CrossRef](#)]

22. Trang, T.N.Q.; Vinh, L.Q.; Doanh, T.T.; Thu, V.T.H. Structure-adjustable colloidal silver nanoparticles on polymers grafted cellulose paper-based highly sensitive and selective SERS sensing platform with analyte enrichment function. *J. Alloys Compd.* **2021**, *867*, 159158. [[CrossRef](#)]
23. Wang, T.; Barveen, N.; Liu, Z.; Chen, C.; Chou, M. Transparent, flexible plasmonic Ag NP/PMMA substrates using chemically patterned ferroelectric crystals for detecting pesticides on curved surfaces. *ACS Appl. Mater. Interfaces* **2021**, *13*, 34910–34922. [[CrossRef](#)]
24. Kong, L.; Huang, M.; Chen, J.; Lin, M. Fabrication of sensitive silver-decorated cotton swabs for SERS quantitative detection of mixed pesticide residues in bitter gourds. *New J. Chem.* **2020**, *44*, 12779–12784. [[CrossRef](#)]
25. Guo, X.; Wang, D.; Han, R. Nafion stabilized Ag nanopillar arrays as a flexible SERS substrate for trace chemical detection. *Mater. Chem. Phys.* **2020**, *252*, 123291. [[CrossRef](#)]
26. Gao, Y.; Hu, Z.; Wu, J.; Ning, Z.; Jian, J.; Zhao, T.; Liang, X.; Yang, X.; Yang, Z. Size-tunable Au@Ag nanoparticles for colorimetric and SERS dual-mode sensing of palmatine in traditional Chinese medicine. *Pharm. Biomed. Anal.* **2019**, *174*, 123–133. [[CrossRef](#)]
27. Jia, X.; Yu, S.; Cheng, C.; Yang, J.; Li, Y.; Wang, S.; Song, H. Ag nanoparticles modified Fe<sub>3</sub>O<sub>4</sub>/reduced graphene oxide and their acetone sensing properties. *Mater. Chem. Phys.* **2022**, *276*, 125378. [[CrossRef](#)]
28. Luo, M.; Zhang, Y.; Zhao, S. Non-Enzymatic Hydrogen Peroxide Sensor Based on Fe<sub>3</sub>O<sub>4</sub>@Polydopamine-Ag Nanocomposite Modified Magnetic Glassy Carbon Electrode. *J. Electrochem. Soc.* **2021**, *168*, 067511. [[CrossRef](#)]
29. Zhang, Q.; Guo, W.; He, L.; He, L.; Chen, Y.; Shen, X.; Wu, D. A new SERS substrate of self-assembled monolayer film of gold nanoparticles on silicon wafer for the rapid detection of polycyclic aromatic hydrocarbons. *Mater. Chem. Phys.* **2020**, *250*, 122994. [[CrossRef](#)]
30. Wang, W.; Li, X.; Yan, Y. Preparation of Au/Fe<sub>3</sub>O<sub>4</sub>/GO composite as SERS substrate and its application in the enrichment and detection for low-concentration pyrene. *Acta Sci. Circumstantiae* **2018**, *38*, 475–483.
31. Jones, C.L.; Bantz, K.C.; Haynes, C.L. Partition layer-modified substrates for reversible surface-enhanced Raman scattering detection of polycyclic aromatic hydrocarbons. *Anal. Bioanal. Chem.* **2009**, *394*, 303–311. [[CrossRef](#)]
32. Olson, L.G.; Uibel, R.H.; Harris, J.M. C18-Modified Metal-Colloid Substrates for Surface-Enhanced Raman Detection of Trace-Level Polycyclic Aromatic Hydrocarbons in Aqueous Solution. *Appl. Spectrosc.* **2004**, *58*, 1394–1400. [[CrossRef](#)] [[PubMed](#)]
33. Costa, J.C.S.; Sant'Ana, A.C.; Corio, P.; Temperini, M.L.A. Chemical analysis of polycyclic aromatic hydrocarbons by surface-enhanced Raman spectroscopy. *Talanta* **2006**, *70*, 1011–1016. [[CrossRef](#)] [[PubMed](#)]
34. Du, J.; Jing, C. Preparation of Fe<sub>3</sub>O<sub>4</sub>@Ag SERS substrate and its application in environmental Cr(VI) analysis. *J. Colloid Interface Sci.* **2011**, *358*, 54–61. [[CrossRef](#)] [[PubMed](#)]
35. Wang, X.; Cheng, H.; Min, Y. Fe<sub>3</sub>O<sub>4</sub>@m-ZrO<sub>2</sub>@Ag ternary magnetic nanocomposites for sensitive SERS sensing and photo-catalytic removal of Cr(VI) and organic dyes. *Compos. Part B Eng.* **2022**, *239*, 109959. [[CrossRef](#)]
36. Wang, X.; Xu, Q.; Hu, X.; Han, F.; Zhu, C. Silver-nanoparticles/graphene hybrids for effective enrichment and sensitive SERS detection of pol-ycyclic aromatic hydrocarbons. *Spectrochim. Acta Part A Mol. Biomol. Spectrosc.* **2020**, *228*, 117783. [[CrossRef](#)] [[PubMed](#)]
37. Fan, M.; Brolo, A.G. Silver nanoparticles self assembly as SERS substrates with near single molecule detection lim-it. *Phys. Chem. Chem. Phys.* **2009**, *11*, 7381–7389. [[CrossRef](#)]
38. Bauer, G.; Hassmann, J.; Walter, H.; Haglmüller, J.; Mayer, C.; Schalkhammer, T. Resonant nanocluster technology—from optical coding and high quality security features to biochips. *Nanotechnology* **2003**, *14*, 1289–1311. [[CrossRef](#)]
39. Du, J.; Xu, J.; Sun, Z.; Jing, C. Au nanoparticles grafted on Fe<sub>3</sub>O<sub>4</sub> as effective SERS substrates for label-free detection of the 16 EPA priority polycyclic aromatic hydrocarbons. *Anal. Chim. Acta* **2016**, *915*, 81–89. [[CrossRef](#)]